

# Horror Image Recognition Based on Context-Aware Multi-Instance Learning

Bing Li<sup>1</sup>, Weihua Xiong<sup>1</sup>, Ou Wu<sup>1</sup>, Weiming Hu<sup>1\*</sup>, Stephen Maybank<sup>2</sup>, Shuicheng Yan<sup>3</sup>

<sup>1</sup>National Laboratory of Pattern Recognition, Institute of Automation, Chinese Academy of Sciences, China

<sup>2</sup>School of Computer Science and Information Systems, Birkbeck College, UK

<sup>3</sup>Department of ECE, National University of Singapore, Singapore

(\*Corresponding Author: wmhu@nlpr.ia.ac.cn)

**Abstract** Horror content sharing on the Web is a growing phenomenon that can interfere with our daily life and affect the mental health of those involved. As an important form of expression, horror images have their own characteristics that can evoke extreme emotions. In this paper, we present a novel context-aware multi-instance learning (CMIL) algorithm for horror image recognition. The CMIL algorithm identifies horror images and picks out the regions that cause the sensation of horror in these horror images. It obtains contextual cues among adjacent regions in an image using a random walk on a contextual graph. Borrowing the strength of the Fuzzy Support Vector Machine (FSVM), we define a heuristic optimization procedure based on the FSVM to search for the optimal classifier for the CMIL. To improve the initialization of the CMIL, we propose a novel visual saliency model based on tensor analysis. The average saliency value of each segmented region is set as its initial fuzzy membership in the CMIL. The advantage of the tensor-based visual saliency model is that it not only adaptively selects features, but also dynamically determines fusion weights for saliency value combination from different feature subspaces. The effectiveness of the proposed CMIL model is demonstrated by its use in horror image recognition on two large scale image sets collected from the Internet.

**Keywords:** horror image recognition, context-aware multi-instance learning, visual saliency

## 1 Introduction

In the past decades, the explosive growth of Web technologies and resources has allowed us to conveniently share texts, images, and videos via the Internet from geographically disparate locations. Meanwhile, the fact that Web content publishing on the Internet lacks clear security standards and

regularizations allows the distribution of many harmful documents dealing with pornography, violence, horror, racism, etc. To prevent people, especially children, from accessing the harmful content on the Internet, many content-based Web filtering systems have been developed [1, 2, 36].

Automatic web filtering is most highly developed for documents with pornographic or violent content; some filtering systems have matured to a point where they are usefully deployed [1, 2, 36]. In comparison, the automatic recognition and filtering of horror content is still being explored [9, 10, 11]. Many psychological and physiological researches have emphasized the severe effects of horror images [3, 4, 5]. Field and Lawson [3] point out that exposure to horror increases behavioral avoidance as well as fears. Ollendick and King [5] also describe an experiment in which 88.8% children ascribe their fear to negative information acquisition. Many governments have taken measures to prevent children from seeing horror films, or even passed laws to limit the public showing of horror films. In the USA, the Motion Picture Association of America (MPAA) categorizes most horror films as “NC-17” (No Children 17 and Under Admitted) [6, 27]. In 2008, the Chinese government banned horror films with violent ghosts, monsters, demons, and other inhuman portrayals [7]. In August 2009, the British Board of Film Censors banned the sale of a Japanese horror DVD because of its psychological harm to audiences [8]. The severity of the effects of horror films makes a horror content filtering system a necessity.

## **1.1 Related Work**

Despite the importance of the horror content filtering, most existing work focuses on horror video recognition. There is, to the best of our knowledge, no specific technique designed for horror image recognition until now. An intuitive and direct solution is to view “horror” as a specific emotion, and to apply general affective image classification methods to recognize it.

Normally, human affects can be represented by different emotional words, such as sadness, excitement, contentment, etc [17, 18]. The basic idea of affective image classification methods is to investigate the relationship between these high level emotional responses and low level image features [12]. The affective image classification methods can be divided into two categories: domain knowledge-based methods and machine learning-based methods [33]. Domain knowledge-based methods build up hierarchical inference models or rules. Most early methods on image emotion analysis belong to this category. Kuroda et al. [34] use the color/texture features of segmented image regions to extract sky/earth/water semantics which are in turn used to produce emotion from the

image. Wang and Yu [13] analyze the emotional meaning embedded in an image through accumulated knowledge and experience. Methods in the machine learning-based category involve the training of mapping functions between low-level features and high-level emotional semantics in a “black box” style. Wang et al. [30] extract image brightness, color temperature, saturation, and contrast features; and then train an emotion classifier using Support Vector Machines (SVM) [19]. Chen et al. [32] propose to recognize the emotion in an image using a Bayesian classifier based on color and texture features. Bianchi-Berthouze [14] extracts a set of features from homogeneous regions in an image and inputs them into neural networks to obtain the emotion information. Fuzzy neural networks are introduced by Guo and Gao [31] into image emotion recognition. Yanulevskaya et al. [15] classify images into 8 emotional categories using an SVM classifier with holistic Weibull and Gabor texture features. Solli and Lenz [16] propose a color-based bag-of-emotions model to retrieve images associated with particular emotions. Liu et al. [33] present a novel affective-probabilistic latent semantic analysis model based on feature’s tensor representation for image emotion classification. Machajdik and Hanbury [17] feed an SVM classifier with a set of effective features inspired by psychology and art theory for affective image classification. Li et al [18] recently propose a novel bilayer sparse representation model for affective image classification by combining global and local features.



**Figure 1. Images with different contextual cues evoke completely different emotions. The images are from the International Affective Picture System (IAPS) dataset [54].**

Although these methods work well in general affective image classification, their performance on horror image recognition is very limited. It is primarily because most existing affective image classification methods try to extract and analyze global features while ignoring the interplay among the regions in an image. However, our observations show that most horror images, in contrast to those positive emotional images including amusement or contentment, generally include two

essential parts: at least one horror region that stimulates a strong emotional response and a certain supporting background. The importance of the context between the two parts is demonstrated by Figure 1. Images including same man but with different objects in his hand create completely different emotions due to different contextual cues; the left image is pleasing while the right one is unsettling. Therefore, an effective classifier for horror image recognition should work on both local regions and their contextual relationships.

## 1.2 Our Work

To circumvent the problems of general affective image classification, we apply multi-instance learning (MIL) [22, 23] to the recognition of horror images. In MIL, an image is viewed as a bag and the regions within it are instances of the bag. Traditional MIL methods treat the instances independently and do not model the relations between different regions [22-24]. This paper proposes a novel context-aware multi-instance learning (CMIL) model for horror image recognition. The experimental results on two large image sets collected from the Internet show that our algorithm outperforms the other competing methods. Our algorithm is original in the following ways:

- We propose a novel context-aware multi-instance learning model (CMIL) that classifies a bag by taking into account both individual instances' labels and their contextual interplay.
- We extend the Fuzzy Support Vector Machine (FSVM) [26] into an effective classifier for the CMIL, referred to as "CMIL-FSVM", that uses a random walk procedure [41] to model the context among instances.
- We present a novel tensor-based visual saliency model to integrate emotional cues adaptively. The resulting visual saliency maps of training images can be used to improve the initialization of the CMIL-FSVM.
- We present a specialized horror image recognition system based on the proposed CMIL model. The system can identify the horror images and the underlying horror regions simultaneously with a set of discriminative visual and emotional features.

The remainder of this paper is organized as follows: Section 2 gives an overview of our work. Section 3 introduces the details of horror image recognition based on CMIL. Section 4 presents an improved initialization of the CMIL-FSVM based on the tensor-based visual saliency model. Section 5 demonstrates the experimental results. Section 6 concludes the paper.

## 2 System Overview

Horror image recognition based on CMIL proceeds in four main stages: bag construction, initial setting, CMIL classifier training, and horror image recognition. Figure 2 gives an overview of our system.

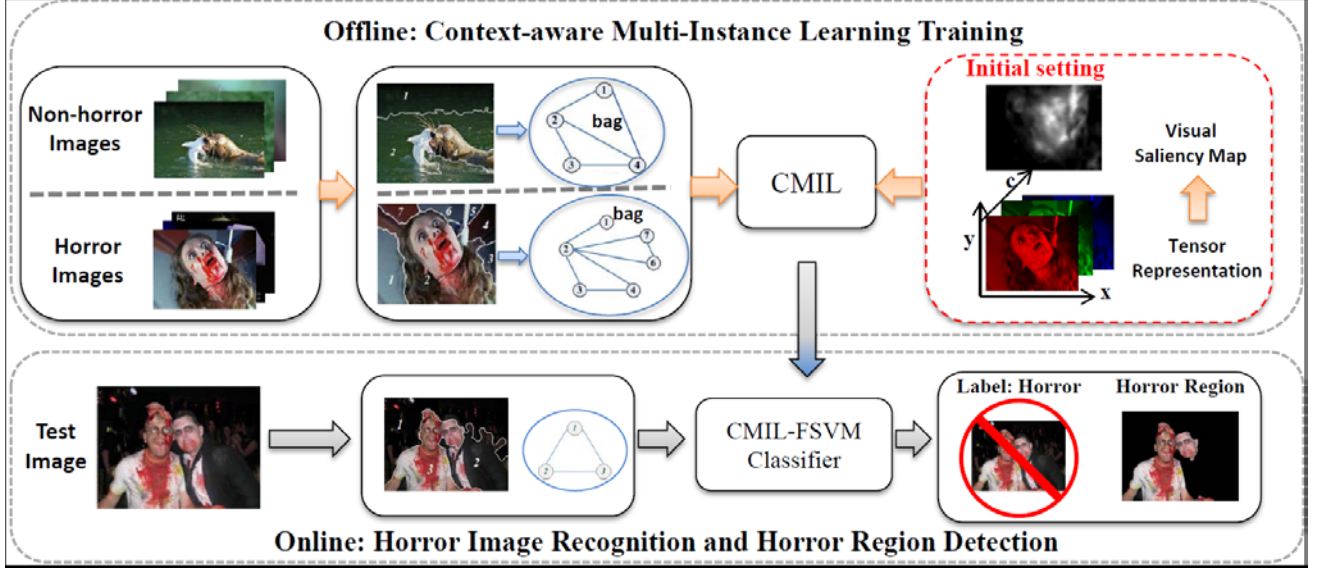


Figure 2. Overview of the proposed framework for horror image recognition.

**Step 1: Bag construction.** We treat each image as a “bag” and all segmented regions in it as “instances”. In each bag, we use an undirected graph to define the contextual relationships between pairs of regions. The vertices of the graph represent the regions. Two vertices are connected by an edge if the corresponding regions are adjacent.

**Step 2: Initial Setting.** In the CMIL-FSVM algorithm, the fuzzy membership of each region in the FSVM for any image is initialized in the training procedure. For the non-horror samples, the initial fuzzy membership of each region is always fixed to be 1. For the horror images, there are two possible strategies for determining the initial fuzzy membership: (1) the fuzzy membership of each region is simply fixed to be a lower value, such as 0.5; or (2) it is gained from the visual saliency map. In the latter strategy, we compute the visual saliency map of each horror image using the proposed tensor-based visual saliency model and set the average saliency value of each region as its initial fuzzy membership.

**Step 3: CMIL classifier training.** We feed the bag and corresponding initial fuzzy membership values, as well as the label of each training image, into the CMIL and apply the proposed CMIL-FSVM algorithm to learn an optimal classifier.

**Step 4: Horror image recognition.** For any test image, we segment it into regions and construct its bag. Then, the CMIL classifier is used to predict whether it is a horror image. If it is predicted to be a horror image, then the classifier further points out the most likely horror region.

### 3 Horror Image Recognition based on CMIL

In the following, we first describe the context-aware multi-instance learning (CMIL) in detail, and then discuss its application to horror image recognition.

#### 3.1 Context-Aware Multi-Instance Learning

##### 3.1.1 Formulation of CMIL

Borrowing the formulation of the traditional MIL [22, 23], we add a new matrix term,  $\mathbf{M}_i$ , into the CMIL definition. The formulation of CMIL is defined as follows: Let  $\mathcal{X}$  denote the instance space. Given a data set  $\{(X_1, \mathbf{M}_1, Y_1), \dots, (X_i, \mathbf{M}_i, Y_i), \dots, (X_N, \mathbf{M}_N, Y_N)\}$  where  $X_i = \{x_{i,1}, \dots, x_{i,j}, \dots, x_{i,n_i}\} \subseteq \mathcal{X}$  is called a bag,  $x_{i,j} \in \mathcal{X}$  is an instance, and  $\mathbf{M}_i$  is an adjacency matrix that specifies a contextual graph to model the relations among the instances in the bag  $X_i$ . The label of the bag  $X_i$  is  $Y_i \in \psi = \{-1, +1\}$ . The underlying label of any instance is not explicitly given. Different from the traditional MIL [22-24], the underlying label of an instance  $x_{i,j}$  in the CMIL is a fuzzy label, defined as  $(y_{i,j}, s_{i,j}) \in \theta_i$ , where  $y_{i,j} \in \psi$  is the class label of  $x_{i,j}$ ,  $0 < s_{i,j} \leq 1$  is the fuzzy membership associated with instance  $x_{i,j}$ , and  $\theta_i$  is the label and fuzzy membership set of the bag  $X_i$ . A hidden contextual score  $E_{i,j}$  is defined for each instance  $x_{i,j}$  in the bag  $X_i$  given the graph adjacency matrix  $\mathbf{M}_i$  and fuzzy membership set  $\theta_i$ . It can be regarded as the tendency of the instance  $x_{i,j}$  towards the positive class considering contextual cues among instances in the bag  $X_i$ . The labels of bags in the CMIL model are determined by the contextual scores and can be interpreted as: If  $Y_i = +1$ , then at least one instance  $x_{i,j} \in \mathcal{X}$  has  $y_{i,j} = +1$  and  $E_{i,j} \geq 0.5$ . If  $Y_i = -1$ , then  $y_{i,j} = -1$  and  $E_{i,j} < 0.5$  for all the instances in bag  $X_i$ .

## (1) Contextual Graph

The contextual graph in the CMIL is designed to represent contextual relationship between any two instances. An example of a contextual graph and its corresponding adjacency matrix  $\mathbf{M}_i$  are shown in Figure 3. Each vertex of the graph corresponds to an instance in the bag  $X_i$ . If there is a direct contextual link between two instances  $x_{i,j}$  and  $x_{i,k}$ , the entry in the adjacency matrix,  $[\mathbf{M}_i]_{j,k}$  is set as 1; otherwise it is set as 0. The details of the graph construction for horror images will be given in Section 3.2.1.

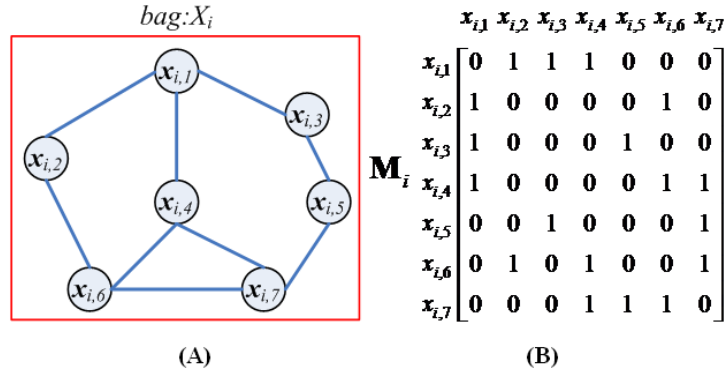


Figure 3. Contextual graph construction: (A) Contextual graph (B) Corresponding adjacency matrix  $\mathbf{M}_i$

## (2) Contextual Score based on Random Walk

An important step in the CMIL is to compute the hidden contextual score  $E_{i,j}$ , for each instance  $x_{i,j}$ , given the contextual graph. The contextual score  $E_{i,j}$  is determined by both the label of  $x_{i,j}$  and the labels of its neighbors. The larger the contextual score  $E_{i,j}$  is, the more possibly positive the instance  $x_{i,j}$  is. To model the contextual scores, we use a random walk on the contextual graph  $\mathbf{M}_i$ . Random walks on graphs [41] are widely used to define the contextual relevance in many practical applications, such as Web page ranking [37, 38], and multimedia retrieval [39, 40].

We first transform the fuzzy membership  $s_{i,j}$  into a corresponding probability value  $p_{i,j}$  that represents the conditional probability  $p(y_{i,j} = 1 | x_{i,j})$  as

$$p_{i,j} = \begin{cases} s_{i,j} & \text{if } y_{i,j} = 1, \\ 1 - s_{i,j} & \text{if } y_{i,j} = -1. \end{cases} \quad (1)$$

Since the probability  $p_{i,j}$  includes no contextual information in the bag  $X_i$ , it can be viewed as the independent score of an instance  $x_{i,j}$ . We concatenate them together and get an independent score vector for the bag  $X_i$  as  $\mathbf{p}_i = [p_{i,1}, p_{i,2}, \dots, p_{i,n_i}]^T$ . The transition probability matrix  $\mathbf{Q}_i = [\mathbf{Q}_i]_{j,k}$  in the random walk is defined as [37, 38]

$$[\mathbf{Q}_i]_{j,k} = \frac{[\mathbf{M}_i]_{j,k} p_{i,k}}{\sum_m [\mathbf{M}_i]_{j,m} p_{i,m}}, \quad (2)$$

where  $[\mathbf{Q}_i]_{j,k}$  is the transition probability from vertex  $x_{i,j}$  to vertex  $x_{i,k}$ . It actually normalizes the independent score value of  $x_{i,k}$  according to all the adjacency vertices of  $x_{i,j}$ .

Given the transition probability matrix  $\mathbf{Q}_i$ , the contextual score  $(E_{i,j})^{t+1}$  of the instance  $x_{i,j}$  at time  $t+1$  is linearly fused by its neighboring vertices' contextual scores at time  $t$  and its own independent score  $p_{i,j}$  [40, 41]:

$$(E_{i,j})^{t+1} = \alpha \sum_k [\mathbf{Q}_i]_{k,j} (E_{i,k})^t + (1-\alpha) p_{i,j}, \quad (3)$$

where  $\alpha$  is the combination weight,  $\sum_k [\mathbf{Q}_i]_{k,j} (E_{i,k})^t$  is the sum score that  $x_{i,j}$ 's neighbors contribute to  $x_{i,j}$ . If we set  $\mathbf{E}_i = [E_{i,1}, E_{i,2}, \dots, E_{i,n_i}]^T$ , Eq. (3) can be rewritten in the matrix form as

$$\mathbf{E}_i^{t+1} = \alpha \mathbf{Q}_i \mathbf{E}_i^t + (1-\alpha) \mathbf{P}_i. \quad (4)$$

Eq. (4) defines a recursive updating of  $\mathbf{E}_i^t$ . It can be shown that the limit  $\mathbf{E}_i = \lim_{t \rightarrow \infty} \mathbf{E}_i^t$  exists [41].

On taking the limit  $t \rightarrow \infty$  in (4), it follows that

$$\begin{aligned} \mathbf{E}_i &= \alpha \mathbf{Q}_i \mathbf{E}_i + (1-\alpha) \mathbf{P}_i, \text{ which reduces to} \\ \mathbf{E}_i &= (1-\alpha)(\mathbf{I} - \alpha \mathbf{Q}_i)^{-1} \mathbf{P}_i. \end{aligned} \quad (5)$$

Given the contextual score  $E_{i,j}$  of each instance  $x_{i,j}$ , the label of each bag in the CMIL can be described in the form of a constraint by

$$Y_i \times \left( \max_{1 \leq j \leq n_i} (E_{i,j}) - 0.5 \right) \geq 0. \quad (6)$$

### 3.1.2 CMIL Classifier Optimization via Fuzzy SVM

The SVM has been extended as the mi-SVM and the MI-SVM to solve MIL problems [24], but the

labels of the instances are always binary. Lin et al. [26] propose the fuzzy SVM (FSVM) in which each input training sample has a fuzzy class membership. In this paper, we propose an extended FSVM, named as CMIL-FSVM, in which the contextual score is added as another constraint.

### (1) Maximum Pattern Margin via FSVM

The basic idea of CMIL-FSVM is to learn a fuzzy classifier in instances space that can predict the label and fuzzy membership of each instance in a bag and then determine the bag's label from these predictions. Let the classification hyperplane in the instance space be  $f(x_{i,j}) = \mathbf{w}^T x_{i,j} + b$  with the parameter  $(\mathbf{w}, b)$  [24]. The optimization objective function of the proposed CMIL-FSVM is obtained by combining the contextual score constraint [26] and the objective function of the FSVM as

$$\begin{aligned} \min_{\mathbf{w}, b} \quad & \frac{1}{2} \|\mathbf{w}\|^2 + C \sum_i \sum_{j=1}^{n_i} s_{i,j} \xi_{i,j}, \\ \text{subject to} \quad & y_{i,j} (\mathbf{w}^T x_{i,j} + b) \geq 1 - \xi_{i,j}, \xi_{i,j} \geq 0, \\ & Y_i \times \left( \max_{1 \leq j \leq n_i} (E_{i,j}) - 0.5 \right) \geq 0, \end{aligned} \quad (7)$$

where  $C$  is a constant and can be regarded as a regularization parameter. If  $s_{i,j}$  in Eq. (7) is small, the effect of the parameter  $\xi_{i,j}$  and the corresponding instance  $x_{i,j}$  is of less importance to the classification hyperplane.

### (2) Optimization Heuristics

The big difficulty to solve Eq. (7) is that, different from the standard classification of the FSVM in which the labels  $y_{i,j}$  and fuzzy membership  $s_{i,j}$  are explicitly predefined in the training procedure, these two terms are not explicitly given out in the CMIL. Inspired by the optimization procedure of the mi-SVM [24], we present a heuristic procedure to minimize the objective function defined in Eq. (7). The optimization procedure includes two major steps: fuzzy classification and label update.

**Step 1: Fuzzy Classification.** Given the hidden label  $y_{i,j}$  and fuzzy membership  $s_{i,j}$  of each instance, the optimization of Eq. (7) is reduced to a quadratic programming problem that can be solved exactly through the FSVM.

**Algorithm 1. Pseudo-code for the CMIL-FSVM optimization heuristics.**

<p><b>Training Procedure</b></p> <p><b>INPUT:</b> All the training bags with corresponding labels as <math>\{(X_1, \mathbf{M}_1, Y_1), \dots, (X_t, \mathbf{M}_t, Y_t), \dots, (X_N, \mathbf{M}_N, Y_N)\}</math>.</p> <p>Initialize <math>y_{i,j} = Y_t</math>, for <math>x_{i,j} \in X_t</math>; <math>s_{i,j} = 1</math>, for <math>x_{i,j} \in X_t</math> and <math>Y_t = -1</math>; <math>s_{i,j} = 0.5</math>, for <math>x_{i,j} \in X_t</math> and <math>Y_t = +1</math>, <math>\Delta s = 0.1</math>.</p> <p>REPEAT</p> <p style="padding-left: 20px;">Compute the classification hyperplane <math>f(x_{i,j})</math> via the FSVM using all the instances.</p> <p style="padding-left: 20px;">Compute outputs <math>f(x_{i,j}) = \mathbf{w}^T x_{i,j} + b</math> for all <math>x_{i,j}</math> in positive bags.</p> <p style="padding-left: 20px;">Compute <math>y_{i,j}</math> and <math>s_{i,j}</math> for all <math>x_{i,j}</math> in positive bags using Eq. (8).</p> <p style="padding-left: 20px;">Set <math>k = 0</math>;</p> <p style="padding-left: 20px;">For (every positive bag <math>X_t</math>)</p> <p style="padding-left: 40px;">Compute <math>E_{i,j}</math> for each instance <math>x_{i,j}</math> in <math>X_t</math> based on Eq. (5).</p> <p style="padding-left: 40px;">Compute <math>j^* = \arg \max_{1 \leq j \leq n_t} (E_{i,j})</math></p> <p style="padding-left: 40px;">If (<math>E_{i,j^*} &lt; 0.5</math>)</p> <p style="padding-left: 60px;">Set <math>s_{i,j^*} = \min(1, s_{i,j^*} + \Delta s)</math>.</p> <p style="padding-left: 60px;">Set <math>k = k + 1</math>.</p> <p style="padding-left: 20px;">END</p> <p style="padding-left: 20px;">END</p> <p>WHILE (<math>k == 0</math> or maximal iteration number is arrived)</p> <p>OUTPUT(<math>\mathbf{w}, b</math>)</p>
<p><b>Test Procedure</b></p> <p><b>INPUT:</b> A test bag <math>X_t</math> and corresponding contextual graph <math>\mathbf{M}_t</math>.</p> <p>Compute outputs <math>f(x_{t,j}) = \mathbf{w}^T x_{t,j} + b</math> for all instances <math>x_{t,j}</math> in <math>X_t</math>.</p> <p>Compute <math>y_{i,j}</math> and <math>s_{t,j}</math> for all instances <math>x_{t,j}</math> in <math>X_t</math>.</p> <p>Compute <math>E_{t,j}</math> for each instance in <math>X_t</math> based on Eq. (5).</p> <p>Compute <math>j^* = \arg \max_{1 \leq j \leq n_t} (E_{t,j})</math></p> <p>IF (<math>E_{t,j^*} \geq 0.5</math>)</p> <p style="padding-left: 20px;">set <math>Y_t = 1</math></p> <p>ELSE</p> <p style="padding-left: 20px;">set <math>Y_t = -1</math></p> <p>END</p> <p>OUTPUT(<math>Y_t</math>)</p>

**Step 2: Label Update.** Once the classification hyperplane has been learnt through FSVM, the hidden label  $y_{i,j}$  and fuzzy membership  $s_{i,j}$  of each instance will be updated based on the hyperplane using Eq.(8).

$$\begin{cases} y_{i,j} = \text{sgn}(f(x_{i,j})), \\ s_{i,j} = \frac{1}{1+e^{-|f(x_{i,j})|}}, \end{cases} \quad (8)$$

where the sigmoid function is widely used to obtain an output from the SVM in the form of probabilities.

After obtaining the classifier during the learning procedure, we can compute the label  $y_{i,j}$  and membership  $s_{i,j}$  of each instance  $x_{i,j}$  in the test bag  $x_i$  using  $f(x_{i,j}) = \mathbf{w}^T x_{i,j} + b$  and Eq. (8). And the label of  $x_i$  can be determined by the labels and memberships of all the instances in  $x_i$ . The implementation details of the CMIL-FSVM are shown in Algorithm 1.

It is worth noting that, during the initialization stage, we pair positive labels of those instances in positive bags with lower fuzzy memberships ( $s_{i,j} = 0.5$ ), and negative labels of those instances in negative bags with higher fuzzy memberships ( $s_{i,j} = 1$ ) so as to make sure that all initial contextual scores of negative bags are less than 0.5. Then, we iteratively adjust the hyperplane by improving the fuzzy memberships of positive instances to ensure that the positive bags satisfy the constraints in Eq. (7).

### 3.1.3 Differences from Other MIL Methods

Many MIL methods have been proposed in the literatures, in which mi-SVM and MI-SVM [24] are widely used. Different from the CMIL that considers contextual cues among instances, these two methods treat all instances from a bag as independently and identically distributed (i.i.d.). The methods that are closer in spirit to our CMIL are miGraph and MIGraph proposed by Zhou et al. [25]. The main difference lies in the definition of the relationship between instances. The miGraph and MIGraph algorithms [25] are essentially graph pattern classifiers. They only consider the global graph structures of a bag and predefine any two instances' relationship based on a  $\epsilon$ -graph that uses the Euclidean distance in a feature space; whereas our CMIL considers contextual cues among instances using a random walk on a spatial adjacency graph. The relationship between any pairs of instances can be dynamically learnt from the training data.

## 3.2 Horror Image Recognition based on CMIL

In this section, we apply the proposed CMIL model to horror image recognition using some effective features.

### 3.2.1 Bag Construction

The first step in the horror image recognition based on CMIL is to construct instances, bags and contextual graphs. The intuitive idea is to treat an image  $I_i$  as a bag and segmented regions  $\{I_{i,1}, I_{i,2}, \dots, I_{i,n_i}\}$  of the image  $I_i$  as instances. Among diverse image segmentation algorithms, the JSEG algorithm [28] is adopted because of its flexibility. After segmentation, we discard the regions whose areas are smaller than 1/40 of the image. Figure 4 gives an example of image segmentation by the JSEG.

The next step is to construct the graph adjacency matrix  $\mathbf{M}$  using the segmented regions in an image. The vertices of the graph represent the image regions and an edge with weight of 1 is defined between any two adjacent regions. An example of a bag and the corresponding graph is shown in Figure 4.

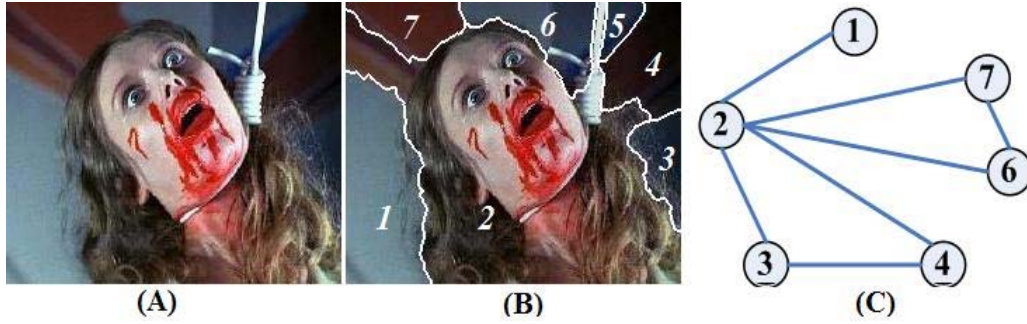


**Figure 4. Bag construction: (A) Original image. (B) Segmentation result. (C) Contextual graph. The 5th region is discarded because it is too small.**

### 3.2.2 Feature Extraction

For each region, three types of features, namely color, color emotion, and texture, are extracted, because they are validated by many affective image classification methods [15, 16, 17].

**Color Feature.** Colors are often used by artists to induce emotional effects. Here we consider image color information in the CIELAB space because it describes color perception more accurately than RGB space [13]. Two feature sets are defined as  $[f_1^k, f_2^k, f_3^k] = [L_k, a_k, b_k]$  and  $[f_4^k, f_5^k, f_6^k] = [|L_k - \bar{L}|, |a_k - \bar{a}|, |b_k - \bar{b}|]$ . The former set is the average of all the pixels' CIELAB values in the  $k^{th}$  region, and the latter set is defined as the difference between averaged pixel value in the  $k^{th}$  region and that of the whole image.

**Color Emotion Feature.** Ou et al. [42] propose a quantitative color emotion model relating the stimulus colorimetry with the emotional response. In detail, they present a three-dimensional color

emotion space with axes representing color activity (  $CA$  ), color weight (  $CW$  ), and color heat (  $CH$  ).

The values of  $CA$ ,  $CW$  and  $CH$  are calculated as follows:

$$\begin{aligned} CA &= -2.1 + 0.06 \left[ (L^* - 50)^2 + (a^* - 3)^2 + \left( \frac{b^* - 17}{1.4} \right)^2 \right]^{1/2}, \\ CW &= -1.8 + 0.04(100 - L^*) + 0.45 \cos(h^* - 100^\circ), \\ CH &= -0.5 + 0.02(C^*)^{1.07} \cos(h^* - 50^\circ), \end{aligned} \quad (9)$$

where  $(L^*, a^*, b^*)$  and  $(L^*, C^*, h^*)$  are the corresponding color values in the CIELAB and CIELCH color spaces for a given RGB color. The average color emotion of the pixels in each region yields a feature vector  $[f_7^k, f_8^k, f_9^k] = [CA_k, CW_k, CH_k]$ , and the difference between it and the whole image yields a second feature vector  $[f_{10}^k, f_{11}^k, f_{12}^k] = [CA_k - \overline{CA}, CW_k - \overline{CW}, CH_k - \overline{CH}]$ .

**Texture Feature.** Geusebroek et al. [43] describe a stochastic texture perception. They show that the distribution of edge responses can be modeled by a Weibull distribution  $wb(z)$  as

$$wb(z) = \frac{\gamma}{\beta} \left( \frac{z}{\beta} \right)^{\gamma-1} e^{-\left( \frac{z}{\beta} \right)^\gamma}, \quad (10)$$

where  $z$  is the edge responses in a single color channel to the Gaussian derivative filter,  $\beta > 0$  is the scale parameter of the distribution and  $\gamma > 0$  is the shape parameter. The parameters of the Weibull distribution completely characterize the spatial structure of the texture [43] and widely used in for texture description [14]. The contrast in an image is represented by  $\beta$ , and the grain size is given by  $\gamma$ . Thus, the  $\beta$  and  $\gamma$  values for the  $x$ -edges and  $y$ -edges in the RGB color channels

for each region yield a 12 dimensional feature vector, as  $[f_{13}^k, f_{14}^k, f_{15}^k, f_{16}^k] = [\gamma_{xR}^k, \beta_{xR}^k, \gamma_{yR}^k, \beta_{yR}^k]$ ,  $[f_{17}^k, f_{18}^k, f_{19}^k, f_{20}^k] = [\gamma_{xG}^k, \beta_{xG}^k, \gamma_{yG}^k, \beta_{yG}^k]$ , and  $[f_{21}^k, f_{22}^k, f_{23}^k, f_{24}^k] = [\gamma_{xB}^k, \beta_{xB}^k, \gamma_{yB}^k, \beta_{yB}^k]$ . In addition, the

texture differences between the current region and the whole image are also used as texture features:

$$[f_{25}^k, f_{26}^k, f_{27}^k, f_{28}^k] = [\gamma_{xR}^k - \gamma_{xR}, \beta_{xR}^k - \beta_{xR}, \gamma_{yR}^k - \gamma_{yR}, \beta_{yR}^k - \beta_{yR}] \quad , \quad [f_{29}^k, f_{30}^k, f_{31}^k, f_{32}^k] = [\gamma_{xG}^k - \gamma_{xG}, \beta_{xG}^k - \beta_{xG}, \gamma_{yG}^k - \gamma_{yG}, \beta_{yG}^k - \beta_{yG}] \quad , \quad \text{and}$$

$$[f_{33}^k, f_{34}^k, f_{35}^k, f_{36}^k] = [\gamma_{xB}^k - \gamma_{xB}, \beta_{xB}^k - \beta_{xB}, \gamma_{yB}^k - \gamma_{yB}, \beta_{yB}^k - \beta_{yB}].$$

The concatenation of all these features yields a feature vector in  $R^{36}$  for each region.

### 3.2.3 Horror Image Recognition Based on CMIL

Given the contextual graph of an image and feature vector of each region in it, we can construct a bag for each image in the CMIL. Now the bag  $X_i$  represents the whole image  $I_i$ ; the instance  $x_{i,j} = [f_1^j, f_2^j, \dots, f_{36}^j] \in R^{36}$  is the feature vector of the  $j^{th}$  region in the image  $I_i$ ;  $\mathbf{M}_i$  is the spatial contextual graph matrix of the image; and the label  $Y_i$  for each image is set to 1 if it is a horror image, and otherwise is set to -1. All the bags of the training images and their corresponding labels are input to the CMIL to learn a classifier using the CMIL-FSVM algorithm. Given a test image, the extracted feature vector of each region and the contextual graph of the image are obtained in the form of a bag. Then, the bag is fed into the CMIL classifier to identify whether it is a horror image. Furthermore, if the test image is judged as a horror image, we consider the region with the highest contextual score to be a horror region in the image.

## 4 Improved CMIL-FSVM by Visual Saliency Map

In Algorithm 1, the memberships of all the instances in the positive bags are simply set to be 0.5 ( $s_{i,j} = 0.5$ ). This initialization may mislead the classifier, because there often exist instances with negative labels or much lower positive memberships in positive bags, such as the background of a horror image. If the CMIL-FSVM is initialized with weak labels and corresponding membership values based on some prior knowledge, the convergence of the classification optimization algorithm may be faster, and a more accurate classifier may be obtained.

Because a horror image always contains one or more popped-out region(s) that is (are) very different from the background in their visual or emotional stimulus. The detection and separation of these salient regions can provide very valuable initialization information to the CMIL-FSVM. In this paper, we propose a simple and effective visual saliency model based on tensor reconstruction, and then discuss how to initialize the CMIL-FSVM using visual saliency maps.

### 4.1 Emotional Attention Mechanism

Much recent psychological research indicates that emotion is of another fundamental importance in the human vision system and produces specific contributions to selective attention [20]. Vuilleumier [21] argues that the amygdala plays a crucial role in providing both direct and indirect signals on sensory pathways, which can influence the representation of emotional events. These modulatory

effects implement specialized mechanisms of “emotional attention” that may supplement visual attention.

In the past decades, many visual saliency computation models [46-52] have been proposed. Most of them follow Koch’s bottom-up saliency map framework [44, 45] that extracts low level visual features and combines the visual saliency values in different feature subspaces to produce the final saliency map [46-52]. Therefore, they have to address two essential questions: (1) find those features with good discriminating power; and (2) determine each feature’s weight in combination.

Although these elaborate methods achieve good performance, they have the following limitations: (1) Most existing visual saliency methods predefine several low level features, such as gray intensity, color channel and local shape orientation, and apply them to all pixels of any input image. These widely-used features may be effective for general visual saliency models; but there is no evidence to show that they are effective for modeling the emotional attention. (2) Most existing methods treat color and texture features separately in visual saliency computation, but research has shown that using color and texture in combination (i.e. color texture) results in better discrimination [55, 56]. (3) Some existing methods fuse saliency maps obtained from different feature subspaces. They predefine a combination weight for the saliency map from each feature subspace. The predefined weights may yield good performance for some images or certain parts of an image; but they cannot always work for all images or for all parts of an image containing different types of scene.

To avoid these limitations, we propose a novel visual saliency map model based on tensor reconstruction that can combine several emotion cues dynamically. In the proposed model, we represent an image in the color emotion space [42] and organize it as a color emotion tensor structure. The first few basis elements in the tensor decompositions of neighboring blocks for each pixel are chosen as features for saliency computation, since they can reveal the most significant information inherent in the surrounding environment. The reconstruction residual error of the pixel’s feature based on these basis elements, which shows whether the pixel includes the similar related features to its neighbors, is used as the visual saliency value. The hypothesis behind the proposed tensor-based saliency map model is that if a pixel is salient, its appearance (color, texture, etc.) and tensor structure will be very different from its neighbors’, so the tensor reconstruction residual using its neighbors will be large. Otherwise, the tensor structure of the pixel is similar to its neighbors’ and the tensor reconstruction residual will be small.

Compared with other existing visual saliency map computation models, our proposed model has



$$\mathcal{M} = \mathcal{Z} \times_1 \mathbf{U}_{block} \times_2 \mathbf{U}_{row} \times_3 \mathbf{U}_{column} \times_4 \mathbf{U}_{color}, \quad (11)$$

where  $\times_1, \times_2, \times_3$  and  $\times_4$  are the  $n$ -mode product operations of the tensor  $\mathcal{Z}$  and matrices  $\mathbf{U}_{row}, \mathbf{U}_{column}$  and  $\mathbf{U}_{color}$  [53]. Here, the core tensor  $\mathcal{Z}$  reflects the interactions among 4 subspaces: the matrix  $\mathbf{U}_{block}$  spans the subspace of block parameter; the matrix  $\mathbf{U}_{row}$  spans the subspace of each block row's parameter, includes correlation between any two rows along all blocks, and represents different texture basis along vertical direction. Similarly, the matrix  $\mathbf{U}_{column}$  spans the subspace of each block column's parameter, includes correlation between any two columns along all blocks, and represents different texture basis along horizontal direction. The matrix  $\mathbf{U}_{color}$  spans the subspace of color emotion parameter and each eigenvector represents one kind of linear transformation of color emotion values.

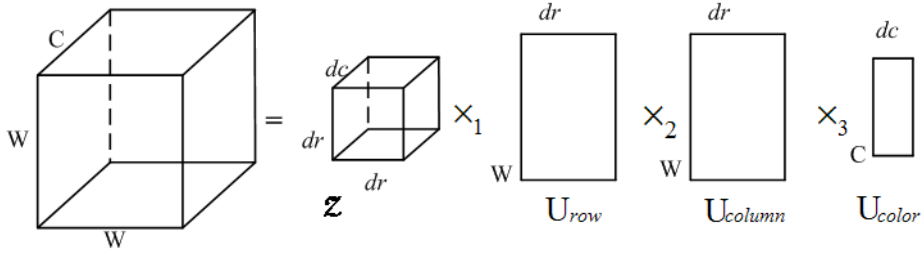


**Figure 6. An example of a 4-order Tucker decomposition viewed from 1<sup>st</sup> Block.**

Since  $\mathbf{U}_{block}$  only represents the correlation among all neighboring blocks, the decomposition output along this order is not considered in the following analysis. So we keep its dimension to be  $16 \times 16$ . For the remaining three orders, we take first  $dr$  eigenvectors of  $\mathbf{U}_{row}$  and  $\mathbf{U}_{column}$  to form the basis matrices  $\mathbf{U}_{row}^{dr}$  and  $\mathbf{U}_{column}^{dr}$  that contain the most important texture energy along vertical and horizontal directions respectively. We also take the first  $dc$  most important linear transformations of the  $\mathbf{U}_{color}$  eigenvectors  $\mathbf{U}_{color}^{dc}$  to emphasize color emotion feature variations. An example of this tensor decomposition is given in Figure 6.

During projection and reconstruction, we represent the center block at location  $\mathbf{q}$  as a 3-order tensor  $\mathcal{T} \in R^{w \times w \times c}$ , then project it using  $\mathbf{U}_{row}^{dr}$ ,  $\mathbf{U}_{column}^{dr}$  and  $\mathbf{U}_{color}^{dc}$ , the projected tensor is  $\mathcal{P} \in R^{dr \times dr \times dc}$ :

$$\mathcal{P} = \mathcal{T} \times_1 (\mathbf{U}_{row}^{dr})^T \times_2 (\mathbf{U}_{column}^{dr})^T \times_3 (\mathbf{U}_{color}^{dc})^T. \quad (12)$$

Then, we get the reconstruction tensor  $\mathcal{T}^R$  of the center block tensor  $\mathcal{T}$  by multiplying the projected  $\mathcal{P}$  with the basis matrices of  $\mathbf{U}_{row}^{dr}$ ,  $\mathbf{U}_{column}^{dr}$  and  $\mathbf{U}_{color}^{dc}$ , as

$$\begin{aligned} \mathcal{T}^R &= \mathcal{P} \times_1 \mathbf{U}_{row}^{dr} \times_2 \mathbf{U}_{column}^{dr} \times_3 \mathbf{U}_{color}^{dc} \\ &= \mathcal{T} \times_1 (\mathbf{U}_{row}^{dr})^T \times_2 (\mathbf{U}_{column}^{dr})^T \times_3 (\mathbf{U}_{color}^{dc})^T \times_1 \mathbf{U}_{row}^{dr} \times_2 \mathbf{U}_{column}^{dr} \times_3 \mathbf{U}_{color}^{dc}. \\ &= \mathcal{T} \times_1 \left( \mathbf{U}_{row}^{dr} (\mathbf{U}_{row}^{dr})^T \right) \times_2 \left( \mathbf{U}_{column}^{dr} (\mathbf{U}_{column}^{dr})^T \right) \times_3 \left( \mathbf{U}_{color}^{dc} (\mathbf{U}_{color}^{dc})^T \right) \end{aligned} \quad (13)$$

After reconstruction, the residual error  $r(\mathbf{q})$  at pixel  $\mathbf{q}$  is computed as

$$r(\mathbf{q}) = \sqrt{\sum_{i=1}^w \sum_{j=1}^w \sum_{k=1}^c (\mathcal{T}_{i,j,k} - \mathcal{T}_{i,j,k}^R)^2}. \quad (14)$$

The result  $r(\mathbf{q})$  is used as the saliency value of the processed pixel. In this way, we approximate the center block's color emotion and texture pattern by the linear sum of the learned patterns of neighbors through tensor reconstruction. Obviously, if the central block has similar features with its neighbors in terms of color emotion and local textures, the principal tensor components gained from neighboring blocks may be similar to those gained from the center block so that the reconstruction error is small, otherwise the reconstruction error is higher and the pixel has a large saliency value.

### 4.2.3 Pyramid Saliency Map Calculation

The pyramid architecture, which is widely used in visual saliency methods, offers a framework for image saliency map calculation with increased resolution quality [52]. We use a pyramid with  $L$  different levels, denoted as  $I^1, I^2, \dots, I^L$ , for the saliency map calculation, where  $I^1$  is the original image and  $I^L$  is the lowest resolution image. The value of  $L$  is determined to be sure that the image's width and height of  $I^L$  are not less than 64 pixels. The normalized saliency map at each level is then resized to match the size of the original image. The values of all the saliency maps at different levels are averaged to gain the final saliency map:

$$SM(\mathbf{q}) = \frac{1}{L} \sum_{l=1}^L \hat{r}_l(\mathbf{q}), \quad (15)$$

where  $SM(\mathbf{q}) \in [0, 1]$  is the final saliency value of pixel  $\mathbf{q}$ ,  $\hat{r}_l(\mathbf{q})$  is the normalized saliency value of pixel  $\mathbf{q}$  in the resized version of the  $l^{th}$  level saliency map.

### 4.3 Initialize of the CMIL with Weak Labels Based on Visual Saliency Map

Using the proposed tensor-based visual saliency map model, we obtain a normalized visual saliency map of each horror image in the training set. As shown in Figure 7, the image regions with high saliency values in a horror image indicate high emotional stimulus. For each positive training image (bag)  $X_i$ , we compute its visual saliency map  $SM_i$ . The average saliency values of all the segmented region (instance) are also computed as  $SM_{i,1}, SM_{i,2}, \dots, SM_{i,n_i}$ . The initial fuzzy membership  $s_{i,j}$  for the instance  $x_{i,j}$  in the bag  $X_i$  is set as:  $s_{i,j} = SM_{i,j}$ , rather than the value of 0.5 used in Algorithm 1.



Figure 7. A horror image with the associated visual saliency map.

## 5 Experiments

To evaluate the performance of the proposed CMIL for horror image recognition, we compared it with other prevailing affective image classification methods as well as some MIL methods on two large scale image sets.

### 5.1 Data Set and Error Measurement

#### 5.1.1 Data Set

Due to a lack of publicly available image sets for horror image recognition, we collected two horror image sets from the Internet. One set includes 1000 horror and non-horror images (referred to as 1000 Horror Image Set). The other one includes 10,000 horror and non-horror images (referred to as 10000 Horror Image Set).

##### (1) 1000 Horror Image Set

This horror image set includes 500 horror images and 500 non-horror images. To collect the horror images, a large number of candidate horror images were first downloaded from three image

search engines (google.com, bing.com, baidu.com) with related query words, such as “horror”, “fear”, “bloody”, and corresponding Chinese words. We invited 7 students in our laboratory to label each image as one of three categories: Non-horror, A little horror, and Horror. Then, we selected 500 images, each of which was labeled as “Horror” by at least 4 users. We also selected 500 non-horror images with different scenes, objects or emotions. These non-horror images include 50 indoor images, 50 outdoor images, 50 human images, 50 animal images, 50 plant images, and 250 images with emotional associations (adorable, amusing, boring, exciting, irritating, pleasing, and surprising). The non-horror images were downloaded from the famous image retrieval system ALIPR, with website (<http://alipr.com/>) using a range of different emotional query words.

In addition, in order to evaluate the performance of the proposed visual saliency map computation model, these 7 students were also required to draw a bounding box around the most salient horror region for each horror image in this set (according to their understanding). The bounding boxes in each image were averaged to get the ground truth of the visual saliency map,  $EM(\mathbf{q})$  [48]:

$$EM(\mathbf{q}) = \{m_{\mathbf{q}} \mid m_{\mathbf{q}} \in [0,1]\}, \text{ where } m_{\mathbf{q}} = \frac{1}{U} \sum_{i=1}^U a_{\mathbf{q}}^i \quad (16)$$

where  $U = 7$  is the number of bounding boxes and  $a_{\mathbf{q}}^i \in \{0,1\}$  is a binary label to indicate whether or not the pixel  $\mathbf{q}$  is inside the bounding box given by the  $i^{\text{th}}$  student.

## (2) 10000 Horror Image Set

The second image set includes 10,000 images, in which there are 5000 horror images and 5000 non-horror images. More than 8,000 candidate horror images were downloaded from a horror image sharing group in a famous image sharing website (flickr.com). The sharing group advises that the users who upload non-horror subject matter will be pulled out. As a result, all the images from this group are horrible. Using the same selection procedure as that in creating 1000 image set, we obtained 5000 horror images after removing duplicates. We also selected 5000 non-horror images from the COREL database [35] which contains a large number of various scenes and is widely used for image understanding research.

### 5.1.2 Error Measurement

For horror image recognition, given the ground truth of a horror image set, referred as  $HS$ , and the recognition results of an algorithm, referred as  $ES$ , the precision ( $pre$ ), recall ( $rec$ ), and  $F_1$

measure defined in Eq. (17) were used to evaluate the recognition performance:

$$pre = \frac{|HS \cap ES|}{|ES|}, \quad rec = \frac{|HS \cap ES|}{|HS|}, \quad F_1 = \frac{2 \times pre \times rec}{pre + rec}. \quad (17)$$

## 5.2 Horror Image Recognition Based on CMIL without Visual Saliency

In this section, we evaluated the performance of the CMIL in terms of horror image recognition without the initialization using the visual saliency map, as shown in Algorithm 1.

We compared the CMIL with some general affective image classification methods: the emotional valence categorization (EVC) algorithm [15], the color based bag-of-emotions (BoE) model [16], the affective-pLSA based method (APLSA) [33] and the bilayer sparse representation-based method (BSR) [18]. Although these methods are not specially designed for horror image recognition, we still used them to classify images as: horror and non-horror. In addition, the leading MIL algorithms, mi-SVM, MI-SVM [24], miGraph, and MIGraph [25], were also applied to horror image recognition for comparison. To fairly compare all these MIL methods, the bag construction and instances' features in MIL methods are the same as those used in our CMIL. Moreover, the Radial Basis Function (RBF) was adopted as kernel functions in the CMIL, mi-SVM, MI-SVM, miGraph, and MIGraph. The parameter  $\alpha$  in Eq. (4) of the CMIL-FSVM was selected from  $\{0.1, 0.3, 0.5, 0.7, 0.9\}$ . The optimal parameters for each algorithm were determined through the 3-cross-validation on the training set in each experiment.

### 5.2.1 Results on 1000 Horror Image Set

The first experiment is on the 1000 horror image set. For each method, we repeated the 3-fold cross validation 10 times and used the average performance of the 10 repeats as the final result.

#### (1) CMIL vs Affective Image Classification Methods

The performance comparisons between the CMIL and other affective image classification methods are shown in Table 1. The experiment results demonstrate that the CMIL outperforms the completing methods. The EVC, BoE and APLSA only use global features for affective image classification. The BSR achieves slightly better performance than the other three affective classification methods due to the fact that the BSR method combines local and global features for classification. However, the BSR is essentially a global method in which it does not consider the contextual cues among regions. These global affective image classification methods tend to misclassify some horror images with large background areas because these areas strongly affect the features on which the classification depends.

**Table 1. Performance comparison with affective image classification methods on the 1000 horror image set.**

Method	<i>Pre</i>	<i>Rec</i>	$F_1$
EVC [15]	0.713	0.612	0.659
BoE [16]	0.722	0.641	0.679
APLSA [33]	0.712	0.636	0.672
BSR [18]	0.713	0.697	0.705
CMIL	0.771	0.763	0.767

**(2) CMIL vs MIL**

We compared the proposed CMIL with 4 leading MIL methods, mi-SVM, MI-SVM [24], miGraph, and MIGraph [25], in terms of horror image recognition on the 1000 horror image set. The mi-SVM and MI-SVM can be viewed as local methods because they work on image regions. The miGraph, MIGraph and CMIL are regarded as contextual methods because they take into account the contextual cues among regions. The experimental results for these methods are listed in Table 2.

**Table 2. Performance comparison with other MIL methods on the 1000 horror image set.**

Method	<i>Pre</i>	<i>Rec</i>	$F_1$
mi-SVM [24]	0.712	0.726	0.719
MI-SVM [24]	0.693	0.707	0.700
miGraph [25]	0.725	0.732	0.728
MIGraph [25]	0.726	0.72	0.723
CMIL	0.771	0.763	0.767

According to Table 2, the proposed CMIL still outperforms other MIL methods. The local MIL methods have slightly higher performance than the global methods [15, 16, 33], but lower performance than the contextual methods. The miGraph and MIGraph algorithms achieve good performance in the image set, but still lower than CMIL. The results show that horror image recognition benefits from exploiting contextual information among the image regions. However, the miGraph and MIGraph methods prefix instances’ relationship using a  $\epsilon$ -graph in feature space and emphasize the global structural of the  $\epsilon$ -graph. This contextual strategy is not very suitable for horror image recognition. In comparison, our CMIL method dynamically learns the contextual cues among regions and focuses on those contextual regions that indicate a horror image.

**5.2.2 Results on 10000 Horror Image Set**

We then conducted experiments on the 10000 image set. Following the same setting in the previous experiment, we obtained performance of each method.

**Table 3. Performance comparison with affective image classification methods on the 10000 horror image set.**

<b>Method</b>	<b><i>Pre</i></b>	<b><i>Rec</i></b>	<b><math>F_1</math></b>
EVC [15]	0.698	0.605	0.648
BoE [16]	0.702	0.632	0.665
APLSA [33]	0.682	0.616	0.647
BSR [18]	0.702	0.653	0.677
CMIL	0.732	0.726	0.729

### (1) CMIL vs Affective Image Classification Methods

Experimental results for the CMIL and for other general affective image classification methods are shown in Table 3. Similar conclusions to those in the previous experiment were obtained. The proposed CMIL method still outperforms the competing affective image classification methods. Interestingly, we found that the precision values of these global methods are slightly higher than their recall values. It proves that some horror images are misclassified as a non-horror because of the background.

**Table 4. Performance comparison with other MIL methods on the 10000 horror image set.**

<b>Method</b>	<b><i>Pre</i></b>	<b><i>Rec</i></b>	<b><math>F_1</math></b>
mi-SVM [24]	0.657	0.695	0.675
MI-SVM [24]	0.649	0.687	0.667
miGraph [25]	0.682	0.691	0.686
MIGraph [25]	0.684	0.701	0.692
CMIL	0.732	0.726	0.729

### (2) CMIL vs MIL

The experimental results of the CMIL and other MIL methods are listed in Table 4. The proposed CMIL still outperforms the MIL methods on this larger set. The miGraph and MIGraph methods still achieve slightly better performance than mi-SVM and MI-SVM. In addition, the precision values of the local methods mi-SVM and MI-SVM are slightly lower than their recall values. It implies that some non-horror images are misclassified as horror images because of their local similarity. The precision and recall values of each contextual algorithm are comparable. It again indicates that contextual cues are helpful for good horror image recognition scheme. When facing the larger scale complex Internet image set, our proposed CMIL still has stable performance.

## 5.3 Horror Image Recognition Based on CMIL with Visual Saliency

We evaluated the proposed CMIL with improved initialization using the tensor-based visual saliency map (denoted as CMIL+TVS). Before evaluating its performance on horror image recognition, we compared the proposed tensor-based visual saliency model with other visual saliency models,

including Itti’s method (Itti) [46], Hou’s method (Hou) [51], Graph-based visual saliency algorithm (GBVS) [50], and Frequency-tuned salient region detection algorithm (FS) [52], in the context of visual saliency map computation.

### 5.3.1 Comparison of Visual Saliency Maps

#### (1) Error Measurement for Visual Saliency Model

Given the ground truth annotation  $EM(\mathbf{q})$  and the computed visual saliency  $SM(\mathbf{q})$  of an image, the precision ( $Spr$ ), recall ( $Sre$ ), and  $F_{0.5}$  measure, which are widely used for visual saliency map evaluation [48], were used for performance comparison:

$$Spr = \frac{\sum_{\mathbf{q}} SM(\mathbf{q})EM(\mathbf{q})}{\sum_{\mathbf{q}} SM(\mathbf{q})}, Sre = \frac{\sum_{\mathbf{q}} SM(\mathbf{q})EM(\mathbf{q})}{\sum_{\mathbf{q}} EM(\mathbf{q})}, F_{0.5} = \frac{(1+0.5) \times Spr \times Sre}{0.5 \times Spr + Sre}. \quad (18)$$

#### (2) Comparison of Visual Saliency Models

There are 3 parameters in the tensor-based saliency map model. The block size, which has little effect because of the pyramid architecture, was set as  $w = 8$ . We set  $dr = 3$  and  $dc = 1$ , meaning that matrices  $\mathbf{U}_{row}^3$ ,  $\mathbf{U}_{column}^3$ , and  $\mathbf{U}_{color}^1$  were used as basis for tensor reconstruction. The Precision ( $Spr$ ), Recall ( $Sre$ ) and  $F_{0.5}$  values of each method are listed in Table 5.

**Table 5 Comparison with existing visual saliency algorithms on the 1000 horror image set**

Method	Precision ( $Spr$ )	Recall ( $Sre$ )	$F_{0.5}$
Itti [46]	0.634	0.505	0.548
Hou [51]	0.644	0.279	0.448
GBVS [50]	0.717	0.512	0.633
FS [52]	0.594	0.683	0.621
<b>Our</b>	<b>0.696</b>	<b>0.801</b>	<b>0.728</b>
Our(RGB)	0.651	0.726	0.674

The performance of our tensor-based model is  $Spr = 0.696$ ,  $Sre = 0.801$  and  $F_{0.5} = 0.728$  respectively, showing that it outperforms the other visual saliency computation methods on this set. Because the other visual saliency methods are designed only from the visual viewpoint, they do not consider the higher emotional stimulus in horror images. In order to test the effectiveness of the color emotion space, we also show the tensor-based model’s results in RGB color space in Table 5 (denoted as Our(RGB)). The lower performance from RGB space indicates that the color emotion space does indeed identify colors with a strong emotional impact and is helpful for emotion-related salient region detection. In addition, the adaptive feature selection and dynamic fusion coefficient embedded

in the proposed tensor-based saliency map model also improve the accuracy of the saliency map. For the qualitative comparison, some saliency maps of the horror images generated by different algorithms are also given in Figure 8. Our proposed method correctly detects the horror regions in almost all of these images.

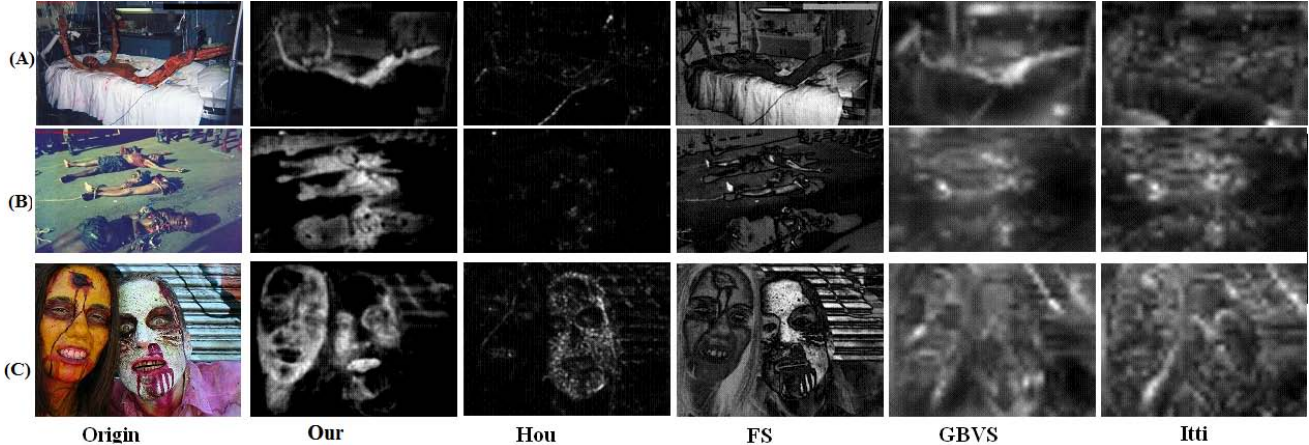


Figure 8. Exemplar saliency maps on horror images produced by different algorithms.

### 5.3.2 Performance Comparison of Horror Image Recognition on 1000 Horror Image Set

In order to further evaluate the effect of the visual saliency map in the CMIL, we compared the CMIL without the visual saliency map (denoted as CMIL) to the CMIL+TVS, as well as the CMIL with the GBVS visual saliency map (denoted as CMIL+GBVS) in terms of horror image recognition. The results are listed in Table 6. The fact that both CMIL+TVS and CMIL+GBVS outperform the CMIL implies that the visual saliency maps do indeed give useful weak labels to the CMIL for improving its performance on horror image recognition. In addition, the CMIL+TVS can achieve a slightly higher  $F_1$  value than the CMIL+GBVS, it is because the GBVS has lower performance on visual salient region detection than the proposed tensor-based model in Table 5.

Table 6. Performance comparison among different CMIL algorithms on the 1000 horror image set.

Method	<i>Pre</i>	<i>Rec</i>	$F_1$
CMIL	0.771	0.763	0.767
CMIL+GBVS	0.781	0.776	0.778
CMIL+TVS	<b>0.809</b>	<b>0.801</b>	<b>0.805</b>

### 5.3.3 Performance Comparison of Horror Image Recognition on 10000 Horror Image Set

We also compared the CMIL, CMIL+TVS and CMIL+GBVS methods on this larger image set. According to the experimental results in Table 7, the CMIL+TVS still outperforms the CMIL+GBVS

and the CMIL.

**Table 7. Performance comparison among different CMIL algorithms on the 10,000 horror image set.**

Method	<i>Pre</i>	<i>Rec</i>	$F_1$
CMIL	0.732	0.726	0.729
CMIL+GBVS	0.731	0.733	0.732
<b>CMIL+TVS</b>	<b>0.786</b>	<b>0.773</b>	<b>0.779</b>

We gave examples of the horror region extraction results of the proposed CMIL+TVS algorithm. Because the instance with the largest contextual score in a bag in the CMIL is most likely to evoke horror emotion, we considered it to be a horror region in the image. Figure 9 gives some horror region extraction results from the CMIL+TVS method. It shows that the CMIL+TVS can correctly identify the underlying horror region of each horror image. Furthermore, the isolated horror regions shown in the second row of Figure 9 evoke almost no feeling of horror. This again indicates that the horror emotion expressed by an image is not evoked by an isolated region but its context.

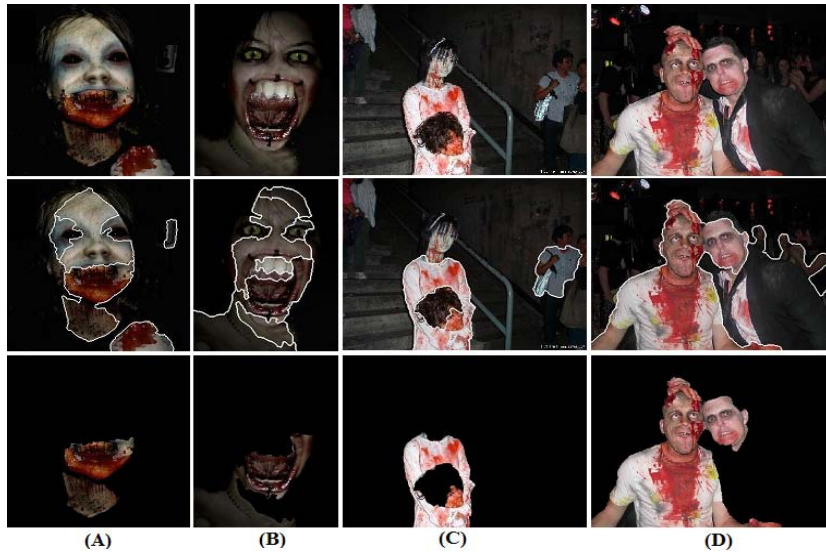


**Figure 9. Examples of horror regions extraction from the CMIL+TVS. The first row contains original images; the images in the second row are segmentation results; the images in the third row are the horror regions extracted by our CMIL algorithm.**

## 6 Conclusions and Future Work

Considering the challenges in horror image recognition from a contextual perspective, we have proposed a novel context-aware multi-instance learning model (CMIL). The CMIL model is based on the fact that the emotion of horror is not evoked by isolated image regions but by the interactions among them. In order to improve the overall performance, the CMIL classifier is initialized using the

visual saliency values that are generated by the proposed tensor-based visual saliency method. The effectiveness of our proposed CMIL framework has been validated on two large scale horror image sets collected from the Internet. Experimental results have showed that the proposed CMIL algorithm is superior to both general affective image classification methods and traditional MIL methods in horror image recognition.

There is still much that has to be done in order to obtain more reliable and general horror image filtering systems. Our future work will focus on the following directions: (1) Exploring more effective emotion-related features for horror image recognition; (2) Integrating the image content analysis with surrounding text tags to filter the horror content on the Web; (3) Investigating online learning scheme so that we can dynamically adjust the classifier as more samples become available.

## ACKNOWLEDGMENTS

This work was supported by the National Nature Science Foundation of China (No. 61370038, 61472421, and 61571045), the 973 Basic Research Program of China (No. 2014CB349303), the Project Supported by CAS Center for Excellence in Brain Science and Intelligence Technology, and Chinese National Programs for High Technology Research and Development (863 Program) (No.2012AA012503 and No. 2012AA012504).

## References

- [1] W. Hu, O. Wu, and Z. Chen. Recognition of pornographic web pages by classifying texts and images. *IEEE Transaction on Pattern Analysis and Machine Intelligence*, 29(6): 1019-1034, 2007.
- [2] M. Hammami, Youssef Chahir, L. Chen. WebGuard: A Web Filtering Engine Combining Textual, Structural, and Visual Content-Based Analysis. *IEEE Transaction on Knowledge and Data Engineering*, pp. 272-284, 2006.
- [3] A. Field, and J. Lawson. Fear information and the development of fears during childhood: effects on implicit fear responses and behavioural avoidance. *Behaviour Research and Therapy*, 41(11): 1277-1293, 2003.
- [4] S. Rachman. The conditioning theory of fear acquisition. *Behaviour Research and Therapy*, 15(5):375-378, 1977.
- [5] T. H. Ollendick and N. J. King. Origins of childhood fears: An evaluation of Rachman's theory of fear acquisition. *Behaviour Research and Therapy*, 29(2):117 -123,1991.
- [6] [http://en.wikipedia.org/wiki/Motion\\_Picture\\_Association\\_of\\_America\\_film\\_rating\\_system](http://en.wikipedia.org/wiki/Motion_Picture_Association_of_America_film_rating_system)
- [7] <http://slashdot.org/article.pl?sid=08/02/16/0654237>
- [8] [http://seattletimes.nwsource.com/html/entertainment/2009687065\\_apeubritainhorrorfilm.html](http://seattletimes.nwsource.com/html/entertainment/2009687065_apeubritainhorrorfilm.html)
- [9] B. Wu, X. Jiang, T. Sun, S. Zhang, X. Chu, C. Shen, and J. Fan. A Novel Horror Scene Detection Scheme on Revised Multiple Instance Learning Model. *Proc. International Conference on Multimedia Modeling*, pp.359-370, 2011.
- [10] J. Wang, B. Li, W. Hu, and O. Wu. Horror Movie Scene Recognition based on Emotional Perception. *Proc. International Conference on Image Processing*, pp.1489-1492, 2010.
- [11] J. Wang, B. Li, W. Hu, and O. Wu. Horror Video Scene Recognition via Multiple-Instance Learning. *Proc. International Conference on Acoustics, Speech, and Signal Processing*, pp. 1325-1328, 2011.
- [12] W. Wang, and Q. He. Survey on Emotional Semantic Image Retrieval. *Proc. International Conference on Image Processing*, pp. 117-120, 2008
- [13] W. N. Wang and Y. L. Yu. Image emotional semantic query based on color semantic description. *Proc. International Conference on Machine Learning and Cybernetics*, pp. 4571-4576, 2005.
- [14] N. Bianchi-Berthouze. K-dime: an affective image filtering system. *IEEE Multimedia*, 10(3):103 - 106, 2003.
- [15] V. Yanulevskaya, J. C. van Gemert and K. Roth. Emotional valence categorization using holistic image features. *Proc.*

*International Conference on Image Processing*, pp. 101-104, 2008

- [16] M. Solli, and R. Lenz. Color based Bag-of-Emotions. *Proc. International Conference on Computer Analysis of Images and Patterns*, pp. 573-580, 2009.
- [17] J. Machajdik and A. Hanbury. Affective Image Classification using Features Inspired by Psychology and Art Theory. *Proc. ACM Conference on Multimedia*, pp. 83-92, 2011
- [18] B. Li, W. Xiong, W. Hu, and X. Ding, Context-aware Affective Images Classification based on Bilayer Sparse Representation. *Proc. ACM Conference on Multimedia*, pp. 721-724, 2012.
- [19] C. Cortes, and V. Vapnik. Support-vector networks. *Machine Learning*, 20(3): 273-297.
- [20] J. D. Eastwood, D. Smilek, and P. M. Merikle. Differential attentional guidance by unattended faces expressing positive and negative emotion. *Perception & Psychophysics*. 63(6): 1004-1013, 2001.
- [21] P. Vuilleumier. How brains beware: neural mechanisms of emotional attention. *TRENDS in Cognitive Sciences*. 9 (12): 585-594, 2005
- [22] Z. H. Zhou. Multi-instance learning: A survey. *Technical Report*, AI Lab, Nanjing University, Nanjing, China, 2004.
- [23] T. G. Dietterich, R. H. Lathrop and T. Lozano-Perez. Solving the multiple-instance problem with axis-parallel rectangles. *Artificial Intelligence*, 89(1-2): 31-71, 1997.
- [24] S. Andrews, I. Tsochantaridis, T. Hofmann. Support vector machines for multiple instance learning. *Proc. Neural Information Processing Systems*, pp. 561-568, 2003.
- [25] Z. Zhou, Y. Sun, and Y. Li. Multi-Instance Learning by Treating Instances As Non-I.I.D. Samples. *Proc. International Conference on Machine Learning*, pp. 1249-1256, 2009.
- [26] C. Lin, and S. Wang. Fuzzy support vector machines. *IEEE Transaction on Neural Networks*, 13(2):464-471, 2002.
- [27] [http://en.wikipedia.org/wiki/List\\_of\\_NC-17\\_rated\\_films](http://en.wikipedia.org/wiki/List_of_NC-17_rated_films).
- [28] Y. Deng, B. S. Manjunath. Unsupervised segmentation of color-texture regions in images and video, *IEEE Transaction on Pattern Analysis and Machine Intelligence*, 23(8): 800-810, 2001.
- [29] C. Galleguillos, and S. Belongie. Context Based Object Categorization: A Critical Survey. *Computer Vision and Image Understanding*, 114(6):712-722, 2010.
- [30] W. Wang, Y. Yu, and S. Jiang. Image retrieval by emotional semantics: A study of emotional space and feature extraction. *Proc. International Conference on Systems, Man, and Cybernetics*, pp. 3534-3539, 2006.
- [31] Y. Guo, and H. Gao. Emotion recognition system in images based on fuzzy neural network and hmm. *Proc. International Conference on Cognitive Informatics*, pp. 73-78, 2006.
- [32] C. H. Chen, M. F. Weng, S. K. Jeng, and Y. Y. Chuang. Emotion-Based Music Visualization Using Photos. *Proc. International Conference on Multimedia Modeling*, pp. 358-368, 2008.
- [33] S. Liu, D. Xu, and S. Feng. Emotion categorization using affective pLSA model. *Optical Engineering*, 49(12): 127201, 2010
- [34] K. Kuroda, and M. Hagiwara. An image Retrieval System by Impression Words and Specific Object Names-IRIS. *Neurocomputing*, 2002, 43:259-276.
- [35] P. Duygulu, K. Barnard, N. Freitas, and D. Forsyth, Object recognition as machine translation: learning a lexicon for a fixed image vocabulary. *Proc. European Conference on Computer Vision*, pp. 97-112, 2002.
- [36] W. Hu, H. Zuo, O. Wu, and Y. Chen. Recognition of Adult Images, Videos, and Web Page Bags. *ACM Transactions on Multimedia Computing, Communications and Applications*, 7S(1):8, 2011.
- [37] S. D. Kamvar, T. H. Haveliwala, C. D. Manning, and G. H. Golub. Extrapolation methods for accelerating page rank computations. *Proc. International World Wide Web Conference*, pp. 261 - 270, 2003.
- [38] A. N. Langville and C. D. Meyer. A survey of eigenvector methods for web information retrieval. *SIAM Review*, 47(1):135-161, 2005.
- [39] W. H. Hsu, L. S. Kennedy, and S. Fu. Chang. Video Search Reranking through Random Walk over Document-Level Context Graph. *Proc. ACM Conference on Multimedia*, pp. 971-980, 2007.
- [40] J. Y. Pan, H. J. Yang, C. Faloutsos, and P. Duygulu. Automatic multimedia cross-modal correlation discovery. *Proc. ACM Conference on Knowledge Discovery and Data Mining*, pp. 653-658, 2004.
- [41] H. Tong, C. Faloutsos, and J. Pan. Fast Random Walk with Restart and Its Applications. *Proc. International Conference on Data Mining*, pp. 613-622, 2006.
- [42] L. Ou, M. Luo, A. Woodcock, and A. Wright. A study of colour emotion and colour preference. part 1: Colour emotions for single colours. *Color Research & Applications*, 29(3): 232-240, 2004.
- [43] J. Geusebroek, and A. Smeulders. A six-stimulus theory for stochastic texture. *International Journal of Computer Vision*, 62(1/2): 7-16, 2005.
- [44] C. Koch and S. Ullman. Shifts in Selection in Visual Attention: Toward the Underlying Neural Circuitry. *Human Neurobiology*, 4(4): 219-27, 1985.
- [45] O. Le Meur, P. Le Callet, D. Barba, and D. Thoreau. A coherent computational approach to model bottom-up visual attention. *IEEE Transaction on Pattern Analysis and Machine Intelligence*, 28(5):802-817, 2006.
- [46] L. Itti, C. Koch, and E. Niebur. A model of saliency-based visual attention for rapid scene analysis. *IEEE Transaction on Pattern Analysis and Machine Intelligence*, 20(11): 1254-1259, 1998
- [47] V. Gopalakrishnan; Y. Hu, and D. Rajan. Salient Region Detection by Modeling Distributions of Color and Orientation. *IEEE Transaction on Multimedia*, 11(5): 892-905, 2009.
- [48] T. Liu, J. Sun, N.N. Zheng, and X. Tang. Learning to detect a salient object. *Proc. IEEE Conference on Computer Vision and Pattern Recognition*, pp. 1-8, 2007
- [49] R. Valenti, N. Sebe, T. Gevers. Image Saliency by Isocentric Curvedness and Color. *Proc. IEEE International Conference on Computer Vision*, pp. 2185-2192, 2009.
- [50] J. Harel, C. Koch, and P. Perona. Graph-based visual saliency. *Proc. Neural Information Processing Systems*, pp. 545-552, 2006.
- [51] X. Hou and L. Zhang. Saliency detection: A spectral residual approach. *Proc. IEEE Conference on Computer Vision and Pattern Recognition*, pp. 1-8, 2007
- [52] R. Achanta, S. Hemami, F. Estrada, and S. Susstrunk. Frequency-tuned salient region detection. *Proc. IEEE Conference on Computer Vision and Pattern Recognition*, pp. 1597-1604, 2009.
- [53] T. G. Kolda and B. W. Bader. Tensor Decompositions and Applications. *SIAM Review*, 51(3):455-500, 2009.

- [54] P. J. Lang, M. M. Bradley and B. N. Cuthbert, International affective picture system (IAPS): affective ratings of pictures and instruction manual, *Technical Report No. A-6*, University of Florida, Gainesville, 2005.
- [55] M. A. Hoang, J. M. Geusebroek, and A. W. M. Smeulders. Color Texture Measurement and Segmentation. *Signal Processing*, 85(2): 265-275, 2005.
- [56] L. Shi, and B. Funt. Quaternion color texture segmentation. *Computer Vision and Image Understanding*, 107(1-2): 88-96, 2007.